Broad-Band Electrical Conductivity of High Density Polyethylene Nanocomposites with Carbon Nanoadditives: Multiwall Carbon Nanotubes and Carbon Nanofibers

A. Linares,*,† J. C. Canalda,† M. E. Cagiao,† M. C. García-Gutiérrez,† A. Nogales,† I. Martín-Gullón,‡ J. Vera,‡ and T. A. Ezquerra†

Instituto de Estructura de la Materia, CSIC, Serrano 119, 28006 Madrid, Spain, and Departamento de Ingeniería Química, Universidad de Alicante, Apdo. 99, 03080 Alicante, Spain

Received March 28, 2008; Revised Manuscript Received July 30, 2008

ABSTRACT: A study is presented of the electrical properties of a series of nanocomposites based on high density polyethylene (HDPE) as a matrix and either carbon nanofiber (CNF) or multiwall carbon nanotube (MWCNT) as a nanoadditive. The measurements of the electrical conductivity over a broad-band of frequencies ($10^{-2} > F/\mathrm{Hz} > 10^{9}$) allow improvement of the description of the electrical properties of polymer nanocomposites based on either carbon nanofibers or carbon nanotubes. Despite the lack of a continuous conducting network between particles at low concentrations, the nanocomposites exhibit a significant dc electrical conductivity due to tunnel conduction. At low nanoadditive concentrations, the frequency dependence of the electrical conductivity is mainly caused by the influence of large polymeric gaps between conducting clusters. As nanoadditive concentration increases, the size of the finite-size cluster tends to increase and the frequency dependence of the conductivity reflects the features of anomalous diffusion in fractal structures, as expected according to percolation theory. A master curve for the electrical conductivity as a function of frequency can be constructed although, for the investigated nanocomposites, this behavior should be contemplated as a working, rather than as a universal, law.

1. Introduction

The electrical properties of composite materials based on polymer matrixes and carbon additives, either particles or fibers, have been intensively studied in the past two decades.[1−3] Depending on the additive concentration, the electrical conductivity of a composite material varies from that of the polymer matrix to that of the carbon additive, due to the formation of a percolative network of the conducting additive at a certain critical concentration.[1−4] Low percolation critical concentrations are highly desirable in order to remain as close as possible to the mechanical properties of the polymer matrix. In the past a lot of attention has been devoted to polymer composites based on carbon black.[1−7] More recently, polymer composites based on carbon nanoadditives, either carbon nanofibers[8,9] (CNF) or carbon nanotubes[10−14] (CNT), have begun to be intensively investigated mainly due to the particular properties of nanocomposites as compared with those of traditional composites. A nanocomposite can be defined as a nanofilled system in which the total interfacial phase becomes the critical parameter instead of the filler concentration.[15] The small diameter and the high aspect ratio of both CNF and CNT favor percolation at very low concentrations.[10−14] Both the direct current (dc) and the alternating current (ac) electrical conductivity of polymer nanocomposites based on multiwall carbon nanotubes (MWCNT) and single wall carbon nanotubes (SWCNT) have been recently discussed[10−14] in a frequency range up to $\approx 10^{6}$ Hz. Different conduction models, including anomalous diffusion in percolating clusters[14] and hopping,[10,13] have been proposed to explain the frequency dependence of the conductivity on CNT nanocomposites. However, a clear picture about the conduction mechanism in nanocomposites is still lacking. In this work, we attempt to shed additional light on this topic by characterizing the electrical conductivity of a polymer nanocomposite in a broader range (up to 10^{9} Hz) than that studied before. The two nanocomposites selected consist of high density polyethylene (HDPE) and either MWCNT or CNF as polymer matrix and nanoadditives, respectively. By comparing the broad-band electrical conductivity of this system precise information about the conduction mechanism in nanocomposites with carbon additives can be extracted.

2. Experimental Section

2.1. Preparation of the Nanocomposites. For this study several nanocomposite samples of HDPE (Repsol-Química, ethylene 1-hexene copolymer (1:1 molar ratio), density = 0.95 g/cm^3) with different amounts of either aligned MWCNT grown on a substrate or CNF grown by the floating catalyst technique were prepared. The diameter of MWCNT and CNF is about 20 and 45 nm, respectively, as characterized by transmission electron microscopy (TEM). The nanocomposites were prepared by intensive mixing of precise amounts of the nanoadditive with HDPE in the molten state ($T = 150$ °C) with a Haake Rheomix equipment of 50 mL of volume mixing chamber, at 20 rpm of shear rate, and during a total time of 40 min. The volume concentration was calculated considering a density of 1.98 g/cm^3 for both CNF and MWCNT. Films of about 1 mm thickness were obtained by compression molding at 140 °C for 2 min, and subsequently cooling down to room temperature under constant pressure.

2.2. Broad-Band Electrical Conductivity. Circular gold electrodes (2 cm in diameter) were deposited onto the surfaces of the film sample. The complex permittivity ε^* of a given sample can be calculated from the measurement of the complex impedance Z^* given by

$$Z^*(\omega) = \frac{U^*(\omega)}{I^*(\omega)} \tag{1}$$

where U^* and I^* are the voltage and current circulating through the sample at a certain angular frequency ω. Once the impedance has been measured, ε^* can be calculated by means of

$$\varepsilon^*(\omega) = \varepsilon' - i\varepsilon'' = \frac{1}{i\omega Z^*(\omega) C_0} \tag{2}$$

where ε' and ε'' are the real and imaginary part of the complex permittivity and C_0 corresponds to capacity of the empty sample

* Corresponding author. E-mail: alinares@iem.cfmac.csic.es.
† Instituto de Estructura de la Materia, CSIC.
‡ Universidad de Alicante.

10.1021/ma801410j CCC: $40.75
Published on Web 09/11/2008

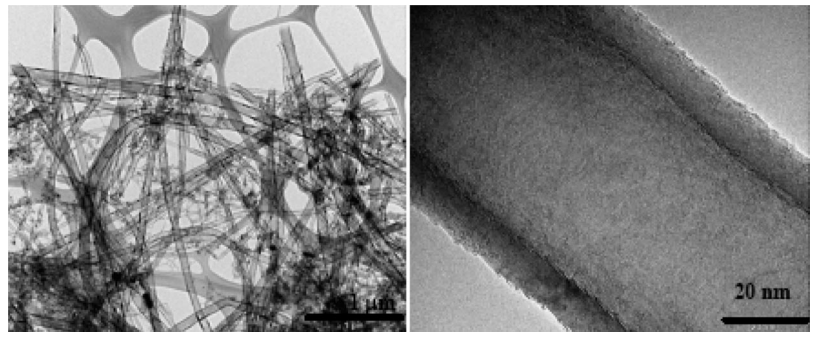

Figure 1. Initial morphology, before mixing, as revealed by TEM of the carbon nanofibers (CNF) at two different magnifications. The scale bars are indicated on the right. The background honeycomb-like structure is due to the TEM grid.

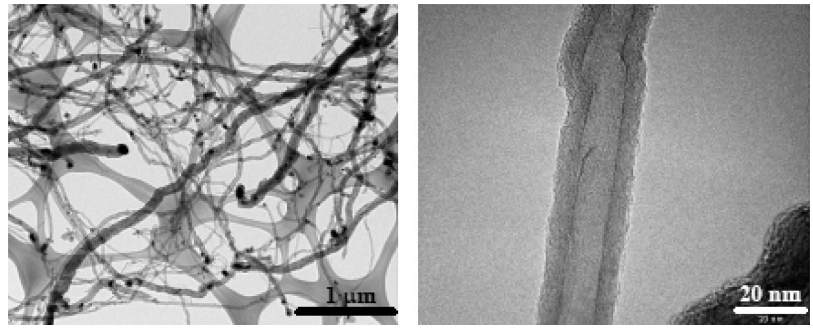

Figure 2. Initial morphology, before mixing, as revealed by TEM of the multiwall carbon nanotubes (MWCNT) at two different magnifications. The scale bars are indicated on the right. The background honeycomb-like structure is due to the TEM grid.

holder. The complex permittivity of the nanocomposites was performed over a frequency window of $10^{-2} < F/\text{Hz} < 10^{9}$ ($F = \omega/2\pi$ is the frequency of the applied electric field). To cover the above frequency interval, two different pieces of equipment were used. In the $10^{-2} < F/\text{Hz} < 10^{6}$ range, a Novocontrol system integrating an ALPHA dielectric interface was employed. In the range $10^{6}-10^{9}$ Hz, dielectric measurements were obtained by means of an HP 4291 coaxial line reflectometer. In this case, the dielectric loss was calculated by measuring the reflection coefficient.[3,5,16] These two instruments were integrated in a Novocontrol broadband dielectric spectrometer. Electrical conductivity was derived by $\sigma(F) = \varepsilon_o 2\pi F\varepsilon''$ where ε_o is the vacuum permittivity.

2.3. Structural Characterization. The dispersion and morphology of the nanoadditives into the matrix were analyzed by transmission electron microscopy (TEM, Jeol JEM 2010). Sections of around 100 nm in thickness were cut by a cryo-ultramicrotomy system. In addition, the morphology and the aspect ratio of the CNF and MWCNT after the nanocomposite processing were observed by scanning electron microscopy (Hitachi S-300N), after the separation polymer−nanoadditive by pyrolysis at 500 °C. At this temperature, all the HDPE evolves as volatiles upon heat treatment, yielding no residue, the CNF and MWCNT remaining. Wide angle X-ray scattering (WAXS) measurements were performed by means of a Seifert XRD 3000 θ/θ diffractometer using Ni-filtered Cu Kα radiation ($\lambda = 0.154$ nm) at a scanning speed of 0.02°/s. Small angle X-ray scattering (SAXS) experiments have been accomplished by a NanoSTAR-U system by Bruker using Cu Kα radiation ($\lambda = 0.154$ nm) equipped with a three pinhole collimation system, cross-couple Göbel mirrors and a Hi-Star multiwire area detector. The SAXS data have been corrected for background scattering by considering the absorption coefficient. Reciprocal space calibration has been done using collagen as standard.

2.4. Mechanical Properties. In order to extract further information about the level of nanoadditive dispersion, the mechanical properties of the samples were characterized by stress−stain tests. Measurements were carried out on dogbone specimens of about 1 mm thickness, conforming to ISO 527-3, using an MTS QT/1 L tensile testing machine. Tests were run at a rate of 10 mm/min, at room temperature.

3. Results and Discussion

3.1. Structure and Morphology of the Nanocomposites. The initial, before mixing, characteristic morphology of the two types of nanoadditive used in this study is shown in Figure 1 and Figure 2 for CNF and MWCNT, respectively. The TEM micrographs are shown at two different magnifications. The initial nanoadditive consists of high aspect ratio tubular structures. At the highest resolutions one clearly sees, in both cases, hollow tubes made of rolled graphene layers, the tube diameters being thicker for CNF than for MWCNT. For CNF the characteristic structure was recently described as made from helix−spiral graphene layers.[17] Figure 3a and Figure 3b show the WAXS diffraction patterns of the nanocomposite with CNF and MWCNT, respectively. The diffracted intensity has been represented as a function of the scattering angle 2θ. HDPE is a semicrystalline polymer, and therefore the diffractograms reveal the presence of two intense maxima at 21.6° and 24° which correspond to the (110) and (200) reflections of the orthorhombic phase of polyethylene.[18] Due to the fact that both CNF and MWCNT consist of several oriented graphene layers, the diffractograms exhibit an additional reflection at 26.2° which corresponds to the (002) reflection from the graphitic layer structure. The fraction of the crystalline phase can be estimated, by using a curve-fitting program, from the ratio of the area below the crystalline peaks to the total area of the diffractogram.[18] Figure 4 shows the crystallinity values of the polymer matrix obtained from the WAXS patterns as a function of additive concentration. The area below the crystalline peak corresponding to the nanoadditive phase has also been represented in Figure 4. The crystallinity of the polymer matrix does not seem to vary significantly by the presence of the nanoadditives. A trend toward a slight decrease of the crystallinity is observed as the amount of nanoadditive increases. The crystallinity difference

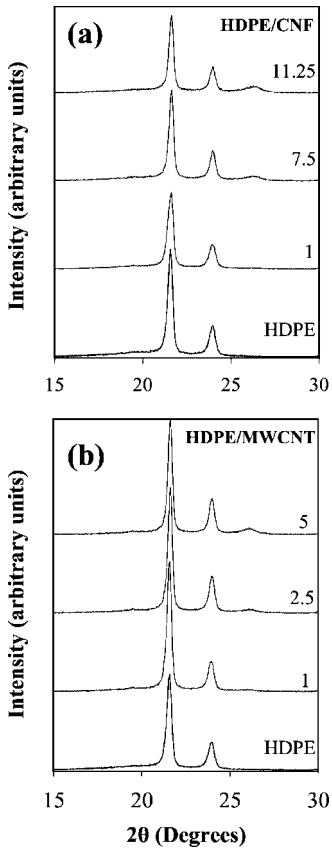

Figure 3. Diffractograms of the HDPE-CNF (a) and HDPE-MWCNT (b) for different concentrations of nanoadditive (labeled on the right).

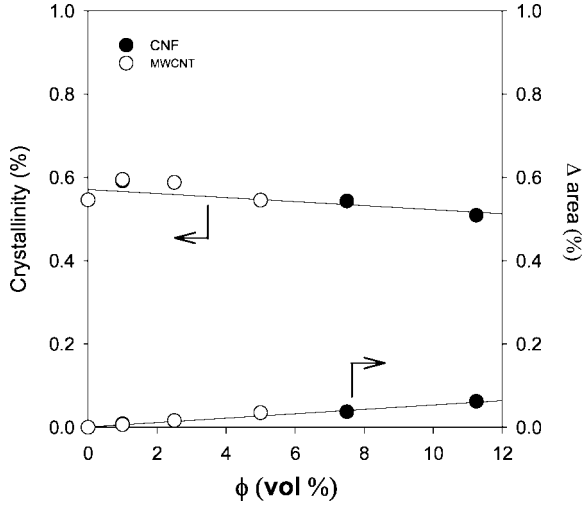

Figure 4. Crystallinity values of the polymer matrix, derived from the analysis of the WAXS patterns, as a function of the nanoadditive concentration: CNF (●) and MWCNT (○). Δ area is the area of the crystalline peak of the nanoadditive phase.

among all samples is smaller than 0.3 vol %. Optical microscopy performed in nanocomposites based on polyethylene and single wall carbon nanotubes has evidenced a dramatic effect on the crystallization kinetics due to the increase of the number of nucleation sites provided by the nanoadditive.[19] However, the impact of the additive on the overall crystallinity levels was not extremely significant.

Figure 5 shows the one-dimensional scattered intensity in the SAXS region as a function of the reciprocal vector $q = 4\pi/\lambda(\sin\theta)$ with 2θ the scattering angle. The one-dimensional

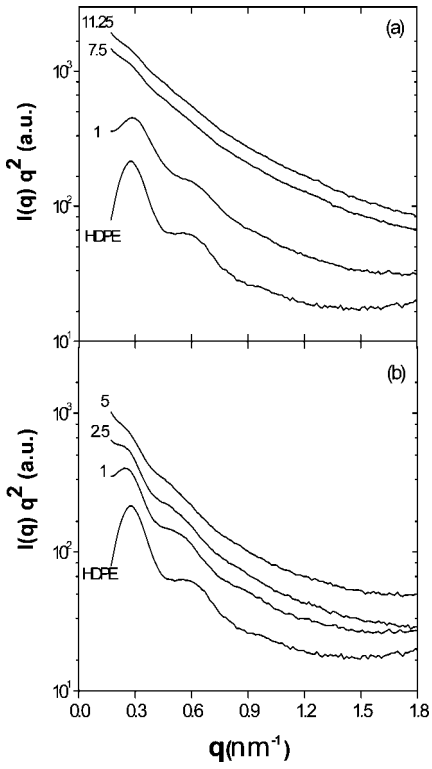

Figure 5. SAXS patterns for HDPE-CNF (a) and HDPE-MWCNT (b) nanocomposites for different nanoadditive volume concentrations (labeled on the figures).

scattering intensity is derived from the azimuthal integration of the two-dimensional scattering images.[20] In all cases, the two-dimensional SAXS images present isotropic patterns. The SAXS of the polymer matrix presents a maximum at around $q_{max} = 0.22$ nm^{-1} accompanied by a higher order maximum at higher q-values. From the main maximum one can obtain the long spacing, $L = 2\pi/q_{max}$, which characterizes the average distance between the gravity center of consecutive crystalline lamellae.[18] For the nanocomposites, the overall scattered intensity increases with nanoadditive concentration due to the scattering of the nanoadditive[20,21] phase. However, the presence of the long spacing maxima is also detectable in the nanocomposites for nanoadditive concentrations smaller than 5 vol %. Samples with high concentrations of nanoadditive present strong SAXS intensity, especially at low q, with a continuous decay related to the fractal structure of the nanoadditive phase.[21] This SAXS intensity completely hides the contribution of the polymer matrix, and therefore, it is not possible to observe the SAXS maximum associated with the periodicity of the semicrystalline structure. However, from the combination of WAXS and SAXS experiments, it is derived that the overall polymer matrix is not significantly modified at the nanostructural level by the presence of the nanoadditives.

Figure 6a and 6b shows TEM micrographies of a nanocomposite with 5 vol % of additives. In Figure 6a, the characteristic MWCNT tubular structures of about some tens of nanometers thick are visible across the sample. On the contrary, Figure 6b shows shorter fiberlike structures, with some fibril fragment around, that indicate a rather wide dispersion of the nanoadditive. In order to investigate the structure of the nanoadditive after the mixing procedure, it was removed by pyrolysis of the polymer matrix. Figure 7a and 7b shows SEM images of the MWCNT and CNF, respectively, extracted from the nanocomposite. While MWCNT exhibit the characteristic fiberlike structure, with an aspect ratio, L/D (with L being the fiber length and D the fiber diameter), ranging from 150 to 400, CNF are

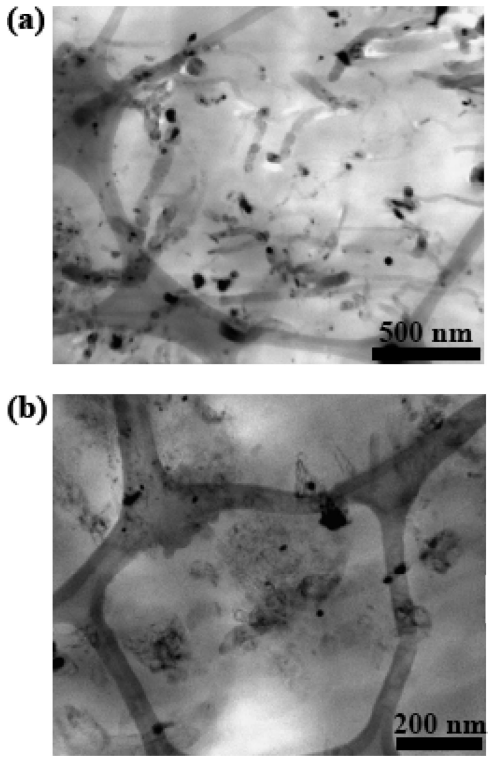

Figure 6. TEM micrographies of HDPE nanocomposites with (a) MWCNT and (b) CNF. The scale bars are indicated on the right. The background honeycomb-like structure is due to the TEM grid.

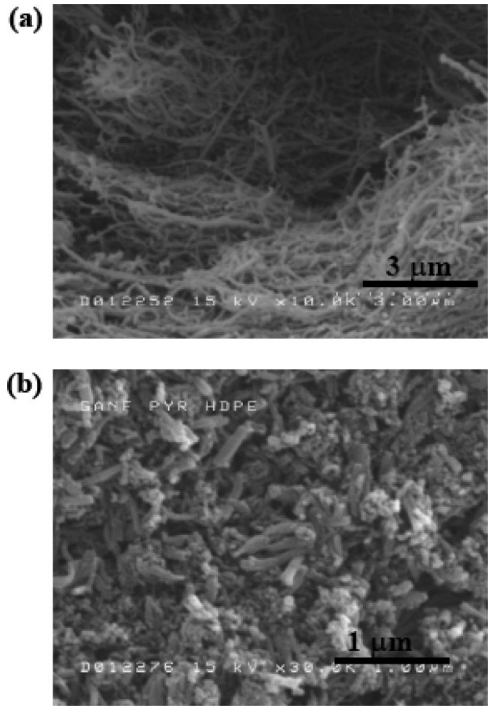

Figure 7. SEM micrographies of (a) MWCNT and (b) CNF after extraction from the nanocomposites. The scale bars are indicated on the bottom right.

characterized by a mixture of short fibers with *L*/*D* aspect ratios ranging from 5 to 10. These images prove that after intensive melt processing nanocomposites based on MWCNT retain much of the characteristic structure of the nanotubes. On the contrary, CNF lose much of the initial fiberlike structure upon high energy mixing with HPDE. It must be emphasized that this effect may have a strong impact on nanoadditive dispersion, as we will show in the next paragraph.

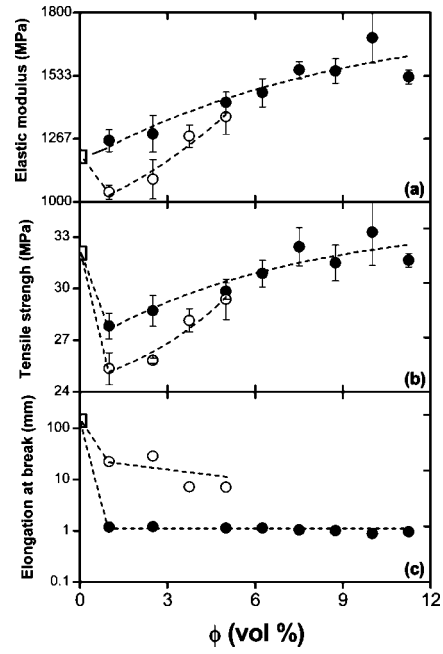

Figure 8. Summary of mechanical properties of HDPE nanocomposites with HDPE (□); CNF (●) and MWCNT (○): (a) elastic modulus, (b) tensile strength and (c) elongation at break. The dashed lines are a guide for the eye.

3.2. Mechanical Properties. Figure 8 shows the elastic modulus, the tensile strength, and the elongation at break for both series of nanocomposites. In spite of the intrinsic mechanical properties of CNT, it has been reported that nanocomposites made out of them frequently exhibit little improvement in mechanical properties at low loading.[22,23] This is the case for HDPE-MWCNT nanocomposites. Data from Figure 8 show that there is an initial decrease in all the mechanical properties investigated for HDPE-MWCNT. However, for HDPE-CNF a very different situation appears. For instance, as shown in Figure 8a, the elastic modulus increases significantly for the complete range of CNF concentration. In the case of MWCNT, an increase with concentration is also observed, but only when the additive content is higher than about 5 vol %, the elastic modulus of both types of composites reaches similar values. This effect is a direct consequence of the different dispersion level of both additives within the polymer matrix. As mentioned in the previous paragraph, CNF break into smaller pieces while MWCNT retain much of their initial aspect ratio. Therefore, dispersion at the nanometer scale is much more difficult to achieve for MWCNT than for CNF nanocomposites. This leads to the apparent surprising effect that, although the intrinsic mechanical properties of MWCNT are greater than those of CNF, the HDPE-CNF nanocomposites exhibit a clear higher enhancement of the mechanical modulus. The other mechanical properties can be interpreted on the same basis.

3.3. Broad-Band Electrical Conductivity. Once a clear picture about the nature of both series of nanocomposites has been established, we can concentrate on the electrical properties of them. The electrical conductivity, $\sigma(F)$, as a function of frequency for samples with different volume concentration, is shown in Figure 9a and 9b for CNF and MWCNT, respectively. For nanoadditive concentrations below 5 vol % for CNF and 1 vol % for MWCNT, $\sigma(F)$ follows a linear dependence with frequency with a slope close to 1, which is characteristic of insulating materials. This is similar to that followed by the HDPE matrix. However, for concentrations higher than the

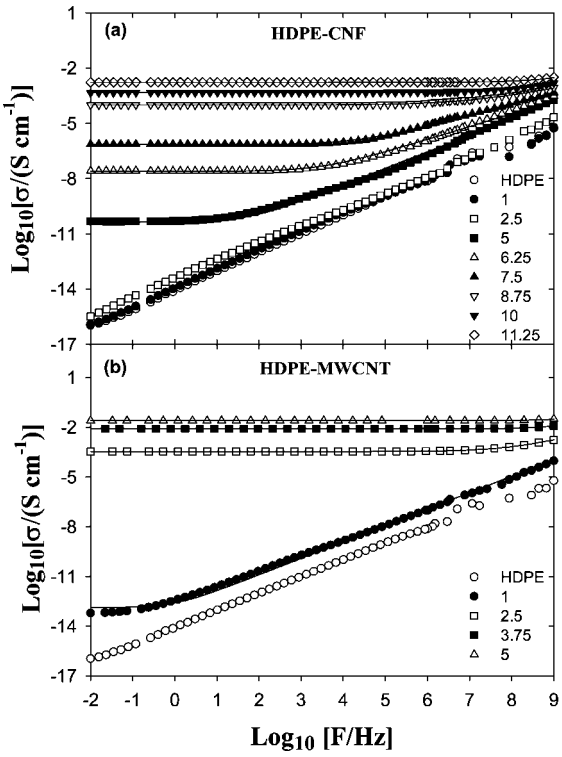

Figure 9. Broad-band electrical conductivity, $\sigma(F)$ as a function of frequency, F, for HDPE-CNF (a) and HDPE-MWCNT (b) nanocomposites with different vol % nanoadditive concentrations (labeled on the right). The continuous lines represent fits according to eq 3.

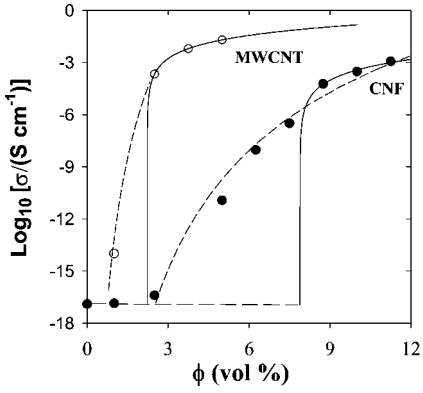

Figure 10. Logarithm of the electrical conductivity versus nanoadditive volume concentration for the CNF (●) and MWCNT (○) nanocomposites. The continuous line is the fitting of eq 5 according to percolation theory. The dashed lines are the predictions according to tunneling conduction.

above referred, values of $\sigma(F)$ adopt a characteristic behavior which can be formally depicted by the so-called universal dynamic response[3,24] described by a law of the type

$$\sigma(F) = \sigma_{dc} + \sigma_{ac} = \sigma_{dc} + AF^S \quad (3)$$

where σ_{dc} is the frequency independent direct current conductivity and $0 < S < 1$. This law introduces a critical frequency, F_c, above which $\sigma(F) = \sigma_{ac} \propto F^S$. The continuous lines in Figure 9 correspond to fits of eq 3 to the experimental data. From these fits the σ_{dc} values can be extracted. The value of the conductivity at the lowest measured frequency (10^{-2} Hz) for the insulating samples has been considered as σ_{dc} for comparative purpose.

3.4. Direct Current Electrical Conductivity. Figure 10 represents the σ_{dc} data as a function of vol % concentration of the nanoadditive for the two systems investigated. The most obvious feature is that the nanocomposite based on MWCNT exhibits significantly higher conductivity values than those of the CNF nanocomposites. In both cases, a characteristic percolative behavior is observed. Initially, for low concentrations, the conductivity remains at the same level as the insulating matrix. At a certain critical concentration around 1 vol % and 3 vol % for MWCNT and CNF nanocomposites, respectively, the conductivity starts a sudden increase.

This effect can be well understood considering the postulated relationship[25] between aspect ratio and critical concentration of the form

$$L/D = 3/\phi_c \quad (4)$$

where ϕ_c is the critical concentration. According to the TEM and SEM images shown in Figure 4, it is evident that the aspect ratio of MWCNT is higher than that of CNF. The dc conductivity above the critical concentration can be analyzed in terms of the percolation theory[4,26] by means of the standard scaling law given by

$$\sigma_{dc} \propto (\phi - \phi_c)^t \quad (5)$$

where t is a critical exponent, which depends on the dimensionality of the system.[4,26] Although the critical concentration, ϕ_c, depends on the lattice in which particles are accommodated, the critical exponent t depends only on the dimensionality of the system.[4] Theoretical calculations, supported by a great amount of experimental observations in both composites with isotropic additives[5] and with fiberlike ones,[10,11,13] propose values of t between 1.6 and 2 for three-dimensional systems. The fitting of eq 5 to the experimental data of Figure 10 provides t-values of around 11 and 4.5 with $\phi_c = 3.2$ vol % and $\phi_c = 1$ vol % for CNF and MWCNT nanocomposites, respectively. This t-value is much beyond the expectations of the percolation theory even for the case in which fiberlike additives are considered.[27,28] In our case t-values within the prediction limits of percolation theory can be obtained by increasing the value of ϕ_c and, therefore, restricting the number of data to be fitted to those with ϕ_c. The continuous lines in Figure 10 show the fittings of eq 5 with $\phi_c = 7.8$ vol % and $t = 2$ for the CNF nanocomposites, and with $\phi_c = 2.2$ vol % and $t = 1.8$ for MWCNT nanocomposites. Percolative behavior in composite materials with high values of the critical exponents has been frequently reported in the literature.[28−30] According to percolation theory the insulator−conductor transition occurs at the critical concentration at which an infinite cluster of connected particles appears. Two particles are said to be connected when they are in physical contact. Electrical conductivities higher than that of the insulating matrix, before a continuous particle network is formed, are expected provided that an interparticle conduction mechanism is present. The existence of tunneling conduction in carbon black composites has been well supported in the literature.[1,5,30−32] More recently also tunneling conduction has been reported for MWCNT and SWCNT nanocomposites.[10,13] In a tunneling process the charge carriers travel through the sample across insulating gaps between particles. The conductivity of a tunnel junction can be described by[1,32]

$$\sigma_{dc} \propto \exp(-Ad) \quad (6)$$

where A is a tunnel parameter and d is the tunnel distance. If a random distribution of particles is assumed, then the mean average distance among particles can be, in a first approximation, assumed to be proportional[33] to $\phi^{-1/3}$. The validity of eq 6, in our case, has been tested by plotting in Figure 11 $\mathrm{Log}_{10}(\sigma_{dc})$ versus $\phi^{-1/3}$. An extended region is observed where a linear dependence is present. The linear dependence described by the continuous lines in Figure 11 has been represented back in Figure 10 by the dashed lines. The good agreement between

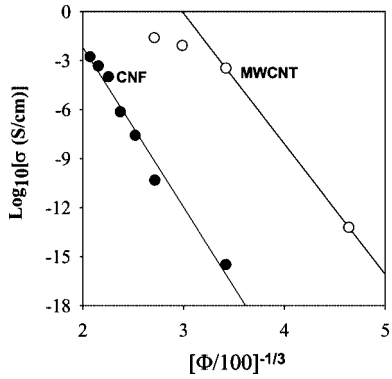

Figure 11. Logarithm of the electrical conductivity versus $(\phi/100)^{-1/3}$. ϕ is the vol % concentration of CNF (●) and MWCNT (○) in the nanocomposites.

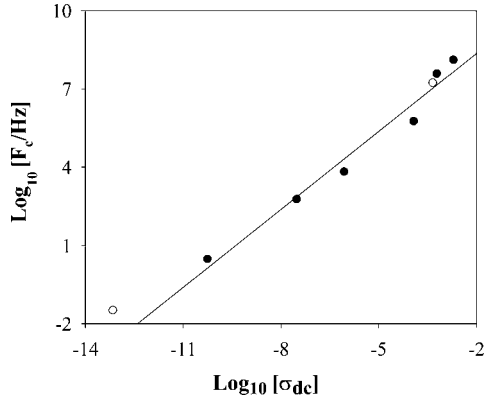

Figure 12. Logarithm of the critical frequency, F_c, versus the logarithm of σ_{dc} for the different nanocomposites based on CNF (●) and MWCNT (○). The continuous line corresponds to the best fitting to eq 7.

the experimental data and the tunneling conductivity suggests that the observed departure, at low concentrations, from the percolation model can be attributed to the existence of tunneling conduction much before particles become physically contacted. The tunneling region is much broader for the CNF nanocomposites. This can be explained by considering eq 4 and by examining the micrographies of Figure 3 and Figure 6. The extended fiberlike structure of MWCNT makes possible the appearance of a conducting network of physically contacting nanotubes at lower concentrations than that needed for CNF nanocomposites.

3.5. Alternating Current Electrical Conductivity. Additionally to the dc conductivity the broad-band measurements provide information about the ac conductivity as described by the frequency dependent part of eq 3. The results of Figure 9 show that the electrical conductivity remains constant until a certain critical frequency, F_c, is reached. For frequencies $F > F_c$ the conductivity exhibits a frequency dependence which, in a first approximation, can be described as $\sigma_{ac} \propto F^S$. The experimental data of Figure 9 also indicate that the higher the dc conductivity the higher is the critical frequency. This effect has been observed for several disordered materials,[34] and it has been described by the following power law

$$F_c \propto \sigma_{dc}{}^{b} \tag{7}$$

where the exponent b takes values close to 1. Figure 12 shows the F_c values as a function of the σ_{dc} ones for the nanocomposites. The F_c data have been calculated for each nanocomposite as that frequency at which a 5% increase in conductivity with respect to the corresponding σ_{dc} value is observed. The power law described is rather well fulfilled with an exponent b

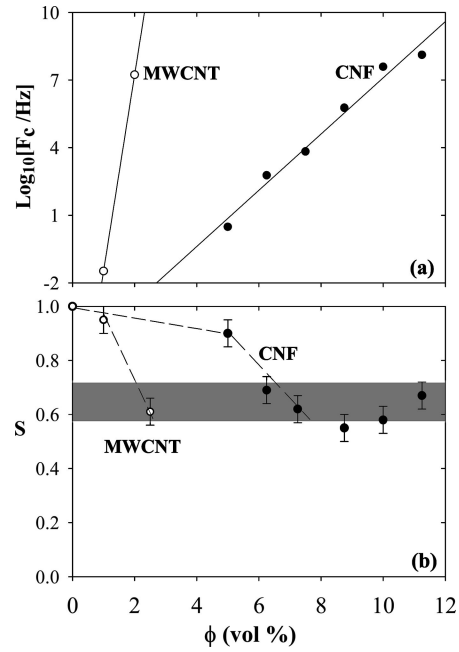

Figure 13. (a) Logarithm of the critical frequency, F_c, and (b) exponent S according to eq 1 as a function of vol % concentration of CNF (●) and MWCNT (○) in the nanocomposites. The gray area in (b) delimits the region described by percolation theory.

≈ 0.99. Figure 13a and Figure 13b show the different values for F_c and S, respectively, as obtained from the fittings of eq 3, as a function of the vol % of additive in the nanocomposite. While the logarithm of F_c increases in a linear fashion with the volume concentration, the S-exponent starts from value $S = 1$, for the insulating specimens, and then a continuous decrease is observed, as the concentration of nanoadditive increases. This behavior has been previously described for SWCNT nanocomposites[13] while for MWCNT nanocomposites only a value of $S \approx 0.92$ was reported.[10] This high value for S was explained as due to hopping transport. This explanation seems to be highly unrealistic considering that carbon nanotubes are, depending on the exact way they are wrapped, either metallic or semiconducting.[35] In both cases electrical conduction takes place through well-defined extended bands and not through localized sites characteristics of hopping.[34] In our case the existence of S-exponents in the range of $S \approx 0.6$ over more than about four decades in frequency is rather well supported for the HDPE-CNF nanocomposites with vol % > 6.25% by the broad-band conductivity measurements (Figure 9 and Figure 13b). The frequency dependence of the electrical conductivity in insulator−conductor composites has been described a long time ago taking into account percolation theory and the geometric nature of the conducting clusters.[36−39] In a percolating system close to the percolation threshold, one assumes to have infinite and finite conducting clusters. A correlation length, ξ, can be defined as the size of the largest finite-size cluster.[40,41] The finite-size clusters have a fractal geometry.[41,42] If one assumes that for a given frequency, F_ξ, the charge carriers scan a distance ξ, then for frequencies $F < F_\xi$ a charge carrier will cover a distance larger than ξ. The frequency dependence of the conductivity has been interpreted as due to the reduction of the length scanned by the charge carriers as frequency increases.[34−38] When this length is smaller than the correlation length, for $F > F_\xi$, then the dynamics of the charge carrier is sensitive to the fractal nature of the conducting clusters. On the basis of these concepts a power law, as that described in eq 3, has been proposed with S-values for three-dimensional materials ranging from $S \approx 0.72$, when polarization effects between particles are considered,[36,38] to $S \approx 0.58$ when anomalous diffusion in fractal clusters is

considered.[37] In Figure 13b, a shaded area has been drawn corresponding to the region in which the expectations of percolation theory are fulfilled. Accordingly, one can delimitate two different regions. First in region I, at low concentrations, nanocomposites exhibit ac conductivities described by eq 3 with high *S*-exponent values $1 > S > 0.7$. Second in region II, at higher concentrations the *S*-exponents are within the limits described by the percolation theory. In order to explain this behavior it is worthwhile to further consider the results of Figure 10 and Figure 11. The dc conductivity data indicate that tunnel conductivity is dominant from low to intermediate nanoadditive concentrations. This fact implies that in region I conduction takes place much before a continuous network of physically connected nanofibers sets on. In this situation the frequency dependence of the electrical conductivity is expected to be caused by the influence of large polymeric gaps between the conducting clusters. Therefore, *S*-exponents close to 1, which is the characteristic exponent of the polymer matrix, are expected. As nanoadditive concentration increases and region II is reached, although tunneling continues being the predominant charge conduction mechanism, the size of the finite-size cluster tends to increase. In this situation, as finite-size clusters are self-similar fractals,[40,41] the frequency dependence of the conductivity reflects, in its *S*-exponent values, the features expected by percolation theory and values $0.58 < S < 0.7$ are measured. As nanoadditive concentration further increases, a continuous network of physically connected nanotubes appears through the sample. In this case, the frequency dependence of the conductivity is much controlled by the nature of the conducting nanoadditive and a weaker frequency dependence of the conductivity is expected since the electrical conductivity of carbon fibers has been shown to be weakly dependent on frequency.[43]

3.6. Master Curve for the Alternating Current Electrical Conductivity. The law describing the frequency dependence of the conductivity, eq 3, has been proposed to be universal for a great amount of disordered materials.[34] This fact is manifested by the possibility to plot the ac conductivity data from a range of experiments on the same plot normalizing conductivity and frequency by an appropriate shift factor. This rule has been shown to be also nearly valid for composite materials based on carbon black,[5] SWCNT[13] and MWCNT.[10] However, as discussed in the previous paragraph, the values of the *S*-exponent may vary with nanoadditive concentration in agreement with previous observations.[13] Therefore, it seems pertinent to check under which conditions the proposed universality is valid for nanocomposites. In order to construct a master curve with the data shown in Figure 9, the conductivity values were normalized by the corresponding σ_{dc} data. Similarly, the frequencies were normalized by the corresponding F_c values. An additional shift in $\mathrm{Log}_{10}(F/F_c)$ of $\approx\pm 0.5$ was allowed in order to correct for data fluctuation in the F_c region. Figure 14 shows the master curve for the conductivity versus frequency data which includes values for the HDPE-CNF and HDPE-MWCNT nanocomposites. Within certain limits a reasonable master curve can be constructed. However, due to the different slopes measured for the different nanoadditive concentrations, the occurrence of this master plot should be considered more as a working rule rather than a true universal behavior.

4. Conclusions

In conclusion, the measurement of the electrical conductivity over a broad-band of frequencies allows one to improve the description of the electrical properties of polymer nanocomposites based on either carbon nanofibers or carbon nanotubes. HDPE-CNF and HDPE-MWCNT nanocomposites investigated here consist, at low nanoadditive concentrations, of isolated conducting regions dispersed within the insulating polymeric matrix. Despite the lack of a continuous conducting network between particles, a significant dc electrical conductivity is observed. A tunnel conduction mechanism is proposed to be predominant in this concentration range. At low nanoadditive concentrations, the frequency dependence of the electrical conductivity is caused by the influence of large polymeric gaps between conducting clusters. As nanoadditive concentration increases, the size of the finite-size cluster tends to increase. In this situation, the frequency dependence of the conductivity reflects the features of anomalous diffusion in fractal structures, as expected according to percolation theory. A master curve can be constructed by appropriate normalization of conductivity and frequency data. However, for the investigated nanocomposites, considering the observed dependence of the exponents describing the ac electrical conductivity, this behavior should be contemplated as a working, rather than as a universal, law.

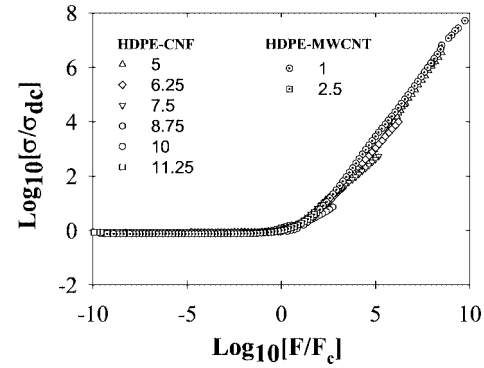

Figure 14. Master curve $\mathrm{Log}_{10}[\sigma/\sigma_{dc}]$ as a function of $\mathrm{Log}_{10}[F/F_c]$ for the HDPE-CNF and HDPE-MWCNT nanocomposites investigated. Different vol % nanoadditive concentrations have been labeled.

Acknowledgment. The authors thank the financial support from the MCYT (grant MAT2005-01768) UE, Spain, for generous support of this investigation. I. Martín-Gullón thanks Prof. R. Andrews for hospitality during his stay in the Center for Applied Energy Research of the University of Kentucky and for providing MWCNT samples.

References and Notes

(1) *Carbon Black Polymer Composites*; Sichel, E. K., Eds.; Marcel Dekker: New York, 1982.
(2) Gul, V. E. In *Structure and properties of conducting polymer composites*; VSP BV: Utrecht, Tokyo, 1996.
(3) *Broadband Dielectric Spectroscopy*; Kremer, F., Schönhals, A., Eds.; Springer: Berlin, 2002.
(4) Stauffer, D. In *Introduction to Percolation Theory*; Taylor & Francis: London, 1985.
(5) Connor, M. T.; Roy, S.; Ezquerra, T. A.; Baltá-Calleja, F. J. *Phys. Rev. B* **1998**, *57*, 2286–2294.
(6) Flandin, L.; Prasse, T.; Schueler, R.; Schulte, K.; Bauhofer, W.; Cavaille, J. Y. *Phys. Rev. B* **1999**, *59*, 14349–14355.
(7) Jäger, K. M.; McQueen, D. H.; Tchmutin, I. A.; Ryvkina, N. G.; Klüppel, M. *J. Phys. D: Appl. Phys.* **2001**, *34*, 2699–2707.
(8) Aleshin, A. N. *Adv. Mater.* **2006**, *18*, 17–27.
(9) Higgins, B. A.; Brittin, W. J. *Eur. Polym. J.* **2005**, *41*, 889–893.
(10) Kilbribe, B. E.; Coleman, J. N.; Fraysse, J.; Fournet, P.; Cadek, M.; Drury, A.; Hutzler, S.; Roth, S.; Blau, W. J. *J. Appl. Phys.* **2002**, *92*, 4024–4030.
(11) Sandler, J. K. W.; Kirk, J. E.; Kinloch, I. A.; Shaffer, M. S. P.; Windle, A. H. *Polymer* **2003**, *44*, 5893–5899.
(12) Pötschke, P.; Dudkin, S. M.; Alig, I. *Polymer* **2003**, *44*, 5023–5030.
(13) Barrau, S.; Demont, P.; Peigney, A.; Laurent, C.; Lacabanne, C. *Macromolecules* **2003**, *36*, 5187–5194.
(14) Nogales, A.; Broza, G.; Roslainec, Z.; Schulte, K.; Šics, I.; Hsiao, B. S.; Sanz, A.; García-Gutiérrez, M. C.; Rueda, D. R.; Domingo, C.; Ezquerra, T. A. *Macromolecules* **2004**, *37*, 7669–7672.
(15) Vaia, R. A.; Wagner, H. D. *Mater. Today* **2004**, *7*, 32–37.
(16) Ezquerra, T. A.; Kremer, F.; Wegner, G. In *Dielectric Properties of Heterogeneous Materials*; Priou, A. , Eds.; Elsevier: Amsterdam, 1992; Vol. *6*.

(17) Vera-Agullo, J.; Varela-Rizo, H.; Conesa, J. A.; Almansa, C.; Merino, C.; Martin-Gullon, I.*Carbon* **2007**, *45*, 2751–2758.
(18) Young, R. J. In *Introduction to Polymers*; Chapman and Hall: London, 1981.
(19) Haggenmueller, R.; Fischer, J. E.; Winey, K. I. *Macromolecules* **2006**, *39*, 2964–2971.
(20) García-Gutiérrez, M. C.; Hernández, J. J.; Nogales, A.; Panine, P.; Rueda, D. R.; Ezquerra, T. A. *Macromolecules* **2008**, *41*, 844–851.
(21) Schaefer, D. W.; Justice, R. S. *Macromolecules* **2007**, *40*, 8501–8517.
(22) Guo, P.; Chen, X.; Gao, X.; Song, H.; Shen, H. *Compos. Sci. Technol.* **2007**, *67*, 3331–3337.
(23) Gojny, F H.; Wichmann, M. H. G.; Fiedler, B.; Bauhofer, W.; Schulte, K. *Composites, Part A* **2005**, *36*, 1525–1535.
(24) Jonscher, A. K. *Nature* **1977**, *267*, 673–679.
(25) Balberg, I.; Anderson, C. H.; Alexander, S.; Wagner, N. *Phys. Rev. B* **1984**, *30*, 3933–3943.
(26) Kirkpatrick, S. *Rev. Mod. Phys.* **1973**, *45*, 574–588.
(27) Carmona, F.; Prudhon, P.; Barreau, F. *Solid State Commun.* **1984**, *51*, 255–257.
(28) Quivy, A.; Deltour, R.; Jansen, A. G. M.; Wyder, P. *Phys. Rev. B* **1989**, *39*, 1026–1030.
(29) Ezquerra, T. A.; Kulescza, M.; Santa Cruz, C.; Baltá-Calleja, F. J. *Adv. Mater.* **1990**, *2*, 597–600.
(30) Ezquerra, T. A.; Kulescza, M.; Baltá-Calleja, F. J. *Synth. Met.* **1991**, *41*−*43*, 915–920.
(31) Sichel, E. K.; Gittleman, J. I.; Sheng, P. *Phys. Rev. B* **1978**, *18*, 5712–5716.
(32) Ryvkina, N.; Tchmutina, I.; Vilcakova, J.; Pelıskova, M.; Saha, P. *Synth. Met.* **2005**, *148*, 141–146.
(33) Boettger, H. , Bryksin, U. V. In *Hopping Conduction in Solids*; Akademie Verlag: Berlin, 1986; pp 108 and 148.
(34) Dyre, J. C.; Schroder, T. B. *Rev. Mod. Phys.* **2000**, *72*, 873–892.
(35) Freitag, M. In *Carbon Nanotubes. Properties and Applications*; Taylor & Francis: New York, 2006; p 83.
(36) Gefen, Y.; Aharony, A.; Alexander, S. *Phys. Rev. Lett.* **1983**, *50*, 77–80.
(37) Laibowitz, R. B.; Gefen, Y. *Phys. Rev. Lett.* **1984**, *53*, 380–383.
(38) Song, Y.; Won-Noh, T.; Lee, S. I.; Gaines, R. *Phys. Rev. B* **1986**, *33*, 904–908.
(39) Mandelbrot, B. In *Les Fractals*; Flammarion: Paris, 1975.
(40) Martin, J. E.; Hurd, J. *J. Appl. Crystallogr.* **1987**, *20*, 61–78.
(41) Kaye, B. H. In *A random Walk through Fractals*; VCH: Weinheim, 1989.
(42) Viswanathan, R.; Heaney, M. B. *Phys. Rev. Lett.* **1995**, *75*, 4433–4436.
(43) Ezquerra, T. A.; Connor, M. T.; Fernandes-Nascimento, J.; Kullescza, M.; Baltá-Calleja, F. J. *Compos. Sci. Technol.* **2001**, *61*, 903–909.

MA801410J